J. Fluid Mech. (1992), *vol.* 237, *pp.* 627–648
Printed in Great Britain

The buoyancy-driven motion of a train of viscous drops within a cylindrical tube

By C. POZRIKIDIS

Department of Applied Mechanics and Engineering Sciences, 0411, University of California, San Diego, La Jolla, CA 92093-0411, USA

(Received 19 March 1990 and in revised form 1 October 1991)

The buoyancy-driven motion of a train of viscous drops settling or rising along the axis of a vertical cylindrical tube is investigated. Under the assumption of creeping flow, the evolution of the drops is computed numerically using a boundary integral method that employs the axisymmetric periodic Green's function for flow in a cylindrical tube. Given the drop volume and assuming that the viscosity of the drops is equal to that of the suspending fluid, the motion is studied as a function of the radius of the tube, the separation between the drops, and the Bond number. Two classes of drops are considered: compact drops whose effective radius is smaller than the radius of the tube, and elongated drops whose effective radius is larger than the radius of the tube. It is found that compact drops may have a variety of steady shapes including prolate and oblate, dimpled tops, and shapes containing pockets of entrained ambient fluid. When the surface tension is sufficiently small, compact drops become unstable, evolving to prolate rings with elongated tails. The terminal velocity of compact drops is discussed and compared with that predicted by previous asymptotic analyses for spherical drops. Steady elongated drops assume the shape of long axisymmetric fingers consisting of a nearly cylindrical main body and two curved ends. Relationships between the terminal velocity of elongated drops, the gap between the drops and the wall of the tube, and the Bond number are established. The results are discussed with reference to previous analyses and laboratory measurements for inviscid bubbles.

1. Introduction

Viscous drops and nearly inviscid bubbles are encountered in a broad range of natural phenomena, biological functions, and engineering applications. Characteristic examples include atmospheric precipitation, underground transport of globular pollutants, dispersion, two-phase flow and heterogeneous mixing in chemical and petroleum engineering processes, and the flow of particulate fluids within conduits and through porous media. The investigation of the mechanics of drops and bubbles has a long record in fluid dynamics, and continues to be a substantial portion of pure and applied research. General reviews on the subject are given by Clift, Grace & Weber (1978) and Rallison (1984).

In one type of classification, previous work may be cast into two categories, one considering motion in a virtually infinite suspending fluid, and the other in a domain of flow which is bounded by a solid boundary or a fluid interface. One of the better studied problems in the second category concerns the motion of a drop in a cylindrical tube (Clift *et al.* 1978, chapter 9). Historically, this problem was first addressed in connection with the air-bubble Cochius viscometer (Faust 1919;

Abrams, Kavanagh & Osmond 1921). Further research was motivated by various applications in industrial and biological systems involving two-phase flow, but also by the abstraction of a cylindrical tube into a modular element of a porous medium or branching network. From an analytical perspective, the geometrical simplicity of the cylindrical tube offers opportunities for accurate analytical and numerical investigations.

Considering, in particular, the behaviour of a drop which is rising or settling due to buoyancy in a vertical cylindrical tube at low Reynolds numbers, we find that the motion will depend primarily on the relative magnitude of the radius of the tube, σ_c, and the equivalent radius of the drop, a. If σ_c is considerably larger than a, the drop will move as if it were immersed in an unbounded suspending fluid. Provided that the drop remains nearly spherical, the flow will be described by the solution of Hadamard and Rybzinsky (see Batchelor 1967). The stability of this motion was investigated by Kojima, Hinch & Acrivos (1984) and Pozrikidis (1990). Physical considerations indicate that as the radius of the tube is decreased, the speed of the drop will be reduced. The effect of decreasing the radius of the tube on the shape and stability of motion of the drop cannot be assessed without carrying out a detailed investigation.

Laboratory observations dating back to the work of Barr (1926) have shown that the behaviour of a drop when σ_c is less than a is not universal, but depends on the value of the tube Bond number $B = |\Delta\rho| g\sigma_c^2/\gamma$, where $\Delta\rho$ is the density difference between the drop and the suspending fluid, g is the acceleration due to gravity, and γ is the surface tension. Bretherton (1961) showed that when $B < 0.842$, the drop will not be able to move, but instead it will push against the wall of the tube forming an upper and a lower static meniscus and halting the fluid flow. At higher values of B, the drop will be able to accommodate itself within the tube, attaining a composite elongated shape that consists of a nearly cylindrical body and two curved ends (Goldsmith & Mason 1962, 1963; O'Brien 1969; Coutanceau & Thizon 1981). Laboratory measurements have shown that the terminal velocity of an elongated drop is nearly independent of its length, as long as this is larger than roughly twice the radius of the cylinder.

Several researchers have carried out theoretical investigations of the low-Reynolds-number buoyancy-driven motion of a drop in a vertical tube. Bretherton (1961) devised an approximate theory for tightly fitting inviscid bubbles. In his analysis, he used the lubrication approximation to describe the flow in the narrow gap between the bubble and the tube, and hydrostatics to describe the top and bottom of the bubble. Finally, he matched the bubble profiles in the two regions using asymptotic methods. His computations produced the critical value $B = 0.842$ mentioned above. Haberman & Sayre (1958) and Hetsroni, Haber & Wacholder (1970) considered the motion of a single small spherical drop using approximate methods. Goldsmith & Mason (1962, 1963) developed a theory to describe the virtually unidirectional flow along the main body of an elongated drop, and derived an equation relating the terminal velocity of the drop to the gap between the drop and the tube. Hyman & Skalak (1972) performed accurate numerical computations of the flow due to a train of spherical drops, considering the motion as a function of the tube radius, drop separation, and ratio between the viscosities of the drop and the suspending fluid. Coutanceau & Thizon (1981) repeated the computations of Hyman & Skalak for the case of solitary drops. More recently, Reinelt (1987) and Mao & Dukler (1990) performed computational studies of the motion of elongated

inviscid drops using finite-difference methods for vanishing and finite Reynolds numbers, respectively.

The objective of this work is to present a numerical study of the creeping, buoyancy-driven motion of a periodic train of viscous drops within a cylindrical tube accounting for the drop deformation. Our computations are aimed to bridge the gap between previous asymptotic analyses, and to extend previous numerical results in three directions. First, we consider periodic trains of drops, and this allows us to examine the combined effect of the presence of the tube and the interactions between multiple drops. Trains of drops arise often in engineering and biomedical applications, e.g. flow of blood cells in the capillaries, and their study is of practical concern. Second, we include the effect of drop deformations; by varying the surface tension, we consider drop shapes ranging from nearly spherical to nearly cylindrical. Third, we consider transient motions in which a train of drops is introduced within the tube, and is allowed to evolve until it reaches either a steady or an asymptotic state. Thus, our results yield information not only on the nature of steady drop shapes but also on the stability of the motion. We shall see that in the absence of surface tension steady drop shapes are not always feasible, and studies of transient motions are necessary in order to establish the behaviour at large times.

Considering a periodic train of drops introduces a new lengthscale which is the separation, L, between two successive drops. When L is infinite, the drops are solitary; in this case, as σ_c becomes much larger than a, the drops behave as if they were immersed in an ambient fluid of infinite extent and their terminal velocity tends to a finite value which is equal or nearly equal to that given by the solution of Hadamard & Rybzinsky (see Batchelor 1967). When L is finite, however, as σ_c is increased, the drops move with an increasingly higher velocity, and in the limit as σ_c becomes infinite, they move at an infinite rate. This behaviour may be explained by noting that far away from a drop, the velocity field due to the drop resembles that due to a point force, and recalling that the velocity field due to an infinite array of point forces is unbounded. This singular behaviour emphasizes the importance of the flow boundaries on the motion of one-dimensional arrays of drops, and calls for an investigation of the combined effects of the drop separation, L, and tube radius, σ_c.

In our formulation, apart from the assumption of Stokes flow which was critically discussed by Bretherton (1961), we introduce two additional assumptions. First, we assume that the motion is axisymmetric, i.e. the drops move precisely along the axis of the vertical tube; the physical relevance of this assumption has been established by previous laboratory observations. Second, we assume that the ratio between the viscosities of the drop and the suspending fluid, λ, is equal to one. This assumption has no physical origin, and is motivated purely by a crucial simplification in our numerical procedure as will be discussed in §2.

At first glance, the choice $\lambda = 1$ might appear quite too specific. Previous work, however, has shown that the dynamics of drops with $\lambda = 1$ is quite similar to that of drops with moderate or small values of λ, roughly less than 5 (Rallison & Acrivos 1978; Pozrikidis 1990; Kennedy 1991). Furthermore, as will be discussed in §4, the behaviour of tightly fitting drops may be shown to be independent of the value of λ. The benefits gained by adopting the choice $\lambda = 1$ were recognized and exploited in several previous computational studies of problems involving convoluted interfaces between viscous fluids (Rallison 1981; Lister 1989).

Our studies rely on numerical solutions that are based on the boundary integral method for Stokes flow (Pozrikidis 1991). Our implementation contains as a key feature the use of the periodic axisymmetric Green's function that vanishes over the

cylindrical wall of the tube. Physically, this Green's function expresses the flow produced by a periodic array of rings of point forces that are coaxial with the tube. The assumption $\lambda = 1$ allows us to express the velocity field simply as a contour integral over the trace of one drop in an azimuthal plane involving the discontinuity in the surface force across the interface, and to formulate the problem in the context of a contour dynamics method for the boundary of one drop. In §2 we shall outline the mathematical formulation and numerical procedure, and in §3 we shall discuss the derivation and computation of the Green's function. In §4 we shall present and discuss the results of our computations.

Before proceeding with our analysis, it is useful to return to the broader framework of our problem and to indicate certain complementary aspects. First, we remark that the problem of the buoyancy-driven motion of a drop in a tube under conditions of inviscid flow has been addressed in numerous laboratory and theoretical studies (see Mao & Dukler 1990 and references cited therein). The complementary problem of motion due to an imposed pressure gradient has been studied on a number of occasions, and recent examples are the finite element computations of Westborg & Hassager (1989) and the boundary integral solutions of Martinez & Udell (1990). The motion of a spherical drop in the presence of surfactants was considered by He, Dagan & Maldarelli (1991).

2. Mathematical formulation and numerical procedure

We consider the gravitational settling of a periodic train of drops of separation L inside a cylindrical tube of radius σ_c, as shown in figure 1. We assume that the drops are moving along the axis of the tube, so the flow is axisymmetric at all times and the net flow rate through a cross-section of the tube is equal to zero. The Reynolds number of the flow inside and outside the drops is assumed to be negligibly small so that the flow is presumed to be in a state of creeping motion. Our objective in this section is to derive an integro-differential equation describing the evolution of the boundary of a drop.

First, it will be necessary to introduce the axisymmetric Green's function of Stokes flow, $\boldsymbol{M}^{\mathrm{TP}}$, where superscript TP stands for *tube-periodic*. Physically,

$$u_\alpha(\boldsymbol{x}) = \frac{1}{8\pi\mu} M^{\mathrm{TP}}_{\alpha\beta}(\boldsymbol{x}, \boldsymbol{x}_0)\, g_\beta \tag{2.1}$$

represents the velocity at the point $\boldsymbol{x} = (x, \sigma)$ produced by an array of rings of point forces of total strength $\boldsymbol{g} = (g_x, g_\sigma)$ placed concentrically within the tube and pointing in the axial or radial direction respectively, where one of the rings is located at the point $\boldsymbol{x}_0 = (x_0, \sigma_0)$; Greek indices stand for x or σ. The derivation and computation of $\boldsymbol{M}^{\mathrm{TP}}$ will be discussed in detail in §3. The net flow rate of (2.1) across any section of the tube is equal to zero.

Following the classical procedure of Rallison & Acrivos (1978), we consider one period of the flow, and write two boundary integral equations for the flow inside and outside a drop using $\boldsymbol{M}^{\mathrm{TP}}$ as the Green's function. Combining these equations, we represent the velocity field in terms of a single-layer potential whose density is proportional to the difference in the surface force across the boundary of a drop, $\Delta \boldsymbol{f}$, and a double-layer integral involving the velocity at the surface of a drop (Pozrikidis 1991, chapter 5). Exploiting the fact that the Green's function is periodic in the x-direction and vanishes over the tube and that the flow rate is equal to zero, and

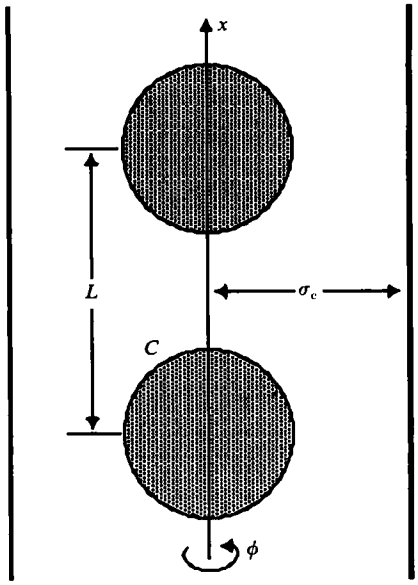

FIGURE 1. Schematic illustration of a train of drops of equivalent radius a separated by a distance L settling under the action of gravity along the centre of a cylindrical tube of radius σ_c.

assuming that the viscosity of the drop, μ, is identical to that of the ambient fluid, we express the velocity field in terms of a single-layer potential that takes the form

$$u_\alpha(\boldsymbol{x}) = -\frac{1}{8\pi\mu}\int_C M^{\mathrm{TP}}_{\alpha\beta}(\boldsymbol{x},\boldsymbol{x}_0)\,\Delta f_\beta(\boldsymbol{x}_0)\,\mathrm{d}S(\boldsymbol{x}_0) \tag{2.2}$$

where C is the trace of the contour of a drop in an azimuthal plane (figure 1). In the case of constant surface tension γ, $\Delta\boldsymbol{f} = (-\Delta\rho\,\boldsymbol{g}\cdot\boldsymbol{x} + \gamma 2k)\,\boldsymbol{n}$, where $\Delta\rho$ is the density difference between the drop and the suspending fluid, k is the mean curvature of the boundary of the drop, and $\boldsymbol{n}$ is the unit normal vector pointing outside the drop.

To compute the evolution of a drop, we represent the trace of the drop in the $\phi = 0$ azimuthal plane using a set of marker points, calculate the velocity at the marker points using the integral representation (2.2), and advance the position of the marker points using the second-order Runge–Kutta method. Details of the numerical implementation are given by Pozrikidis (1990).

Our problem involves two physical constants: the surface tension, γ, and the density difference, $\Delta\rho$; and three lengthscales: the radius of the cylinder, σ_c, the equivalent spherical radius of the drop, $a = (3V/4\pi)^{\frac{1}{3}}$ where V is the volume of a drop, and the separation between two successive drops, L. In our computations, we nondimensionalize all variables using as a characteristic length a, velocity $a^2\Delta\rho g/\mu$, and stress $a\Delta\rho g$. Thus, we consider the motion as a function of the geometric ratios L/a, σ_c/a and the inverse Bond number $\Gamma = \gamma/a^2\Delta\rho g$.

All calculations described in §4 were performed on a SUN-4/60 Sparc Station. A complete transient computation beginning with a spherical initial shape required between 5 and 10 hours of CPU time. Continuation with respect to all parameters was used in order to reduce the time necessary to arrive at a steady shape. In all cases, the change in the volume of a drop, an index of the accuracy of the calculations, was less than 0.5% through the completion of a computation.

3. Computation of the Green's function

In this section we discuss the derivation and computation of the periodic axisymmetric Green's function $\boldsymbol{M}^{\mathrm{TP}}$ associated with an infinite array of rings of point forces separated by a distance L, placed coaxially within a cylindrical tube of radius σ_{c}.

We build the Green's function $\boldsymbol{M}^{\mathrm{TP}}$ in two steps. First, we introduce the axisymmetric Green's function $\boldsymbol{M}^{\mathrm{T}}$ expressing the flow due to a ring of point forces coaxially placed within a cylindrical tube (Tözeren 1984). By definition, $\boldsymbol{M}^{\mathrm{T}}$ is required to vanish when $\sigma = \sigma_{\mathrm{c}}$. It will be convenient to decompose $\boldsymbol{M}^{\mathrm{T}}$ into the free-space component, $\boldsymbol{M}^{\mathrm{R}}$, and a complementary component, $\boldsymbol{M}^{\mathrm{C}}$, writing $\boldsymbol{M}^{\mathrm{T}} = \boldsymbol{M}^{\mathrm{R}} + \boldsymbol{M}^{\mathrm{C}}$. The free-space component $\boldsymbol{M}^{\mathrm{R}}$ expresses the flow due to a ring of point forces in an infinite fluid and is given by

$$\left.\begin{aligned} M^{\mathrm{R}}_{xx} &= 2k\left(\frac{\sigma_0}{\sigma}\right)^{\frac{1}{2}}\left(F+\frac{\hat{x}^2}{r^2}E\right), \quad M^{\mathrm{R}}_{x\sigma} = -k\frac{\hat{x}}{(\sigma_0\sigma)}\left[F-(\sigma^2-\sigma_0^2+\hat{x}^2)\frac{E}{r^2}\right], \\ M^{\mathrm{R}}_{\sigma x} &= k\frac{\hat{x}}{\sigma}\left(\frac{\sigma_0}{\sigma}\right)^{\frac{1}{2}}\left[F+(\sigma^2-\sigma_0^2-\hat{x}^2)\frac{E}{r^2}\right], \\ M^{\mathrm{R}}_{\sigma\sigma} &= \frac{k}{\sigma_0\sigma}\left(\frac{\sigma_0}{\sigma}\right)^{\frac{1}{2}}\left[(\sigma_0^2+\sigma^2+2\hat{x}^2)F-(2\hat{x}^4+3\hat{x}^2(\sigma_0^2+\sigma^2)+(\sigma^2-\sigma_0^2)^2)\frac{E}{r^2}\right], \end{aligned}\right\} \tag{3.1}$$

where $\hat{x} = x - x_0$, $r^2 = \hat{x}^2 + (\sigma - \sigma_0)^2$, and F and E are the complete elliptic integrals of the first and second kind with argument k^2, where

$$k = \frac{2(\sigma\sigma_0)^{\frac{1}{2}}}{[\hat{x}^2+(\sigma+\sigma_0)^2]^{\frac{1}{2}}}.$$

The complementary component $\boldsymbol{M}^{\mathrm{C}}$ was derived by Tözeren in the form of inverse Fourier transforms as

$$\left.\begin{aligned} M^{\mathrm{C}}_{xx} &= \sigma_0\int_0^\infty \begin{bmatrix} tI_0(\omega) \\ \omega I_1(\omega)+2I_0(\omega)\end{bmatrix}\cdot \boldsymbol{A}_x \cos(\hat{x}t)\,\mathrm{d}t, \\ M^{\mathrm{C}}_{x\sigma} &= \sigma_0\int_0^\infty \begin{bmatrix} tI_0(\omega) \\ \omega I_1(\omega)+2I_0(\omega)\end{bmatrix}\cdot \boldsymbol{A}_\sigma \sin(\hat{x}t)\,\mathrm{d}t, \\ M^{\mathrm{C}}_{\sigma x} &= \sigma_0\int_0^\infty \begin{bmatrix} tI_1(\omega) \\ \omega I_0(\omega)\end{bmatrix}\cdot \boldsymbol{A}_x \sin(\hat{x}t)\,\mathrm{d}t, \\ M^{\mathrm{C}}_{\sigma\sigma} &= -\sigma_0\int_0^\infty \begin{bmatrix} tI_1(\omega) \\ \omega I_0(\omega)\end{bmatrix}\cdot \boldsymbol{A}_\sigma \cos(\hat{x}t)\,\mathrm{d}t, \end{aligned}\right\} \tag{3.2}$$

where $\omega = t\sigma$. The vectors $\boldsymbol{A}_x$ and $\boldsymbol{A}_\sigma$ are functions of $\omega_0 = t\sigma_0$, $\omega_{\mathrm{c}} = t\sigma_{\mathrm{c}}$, and t, and arise as solutions to the linear system

$$\begin{bmatrix} tI_0(\omega_{\mathrm{c}}) & \omega_{\mathrm{c}}I_1(\omega_{\mathrm{c}})+2I_0(\omega_{\mathrm{c}}) \\ tI_1(\omega_{\mathrm{c}}) & \omega_{\mathrm{c}}I_0(\omega_{\mathrm{c}})\end{bmatrix}\cdot \boldsymbol{A}_\alpha = 4\boldsymbol{B}_\alpha, \tag{3.3}$$

$$\left.\begin{aligned} \boldsymbol{B}_x(\omega_{\mathrm{c}},\omega_0) &= \begin{bmatrix} B_{xx} \\ B_{x\sigma}\end{bmatrix} = \begin{bmatrix} -2K_0(\omega_{\mathrm{c}})+\omega_{\mathrm{c}}K_1(\omega_{\mathrm{c}}) & -K_0(\omega_{\mathrm{c}}) \\ -\omega_{\mathrm{c}}K_0(\omega_{\mathrm{c}}) & K_1(\omega_{\mathrm{c}})\end{bmatrix}\cdot\begin{bmatrix} I_0(\omega_0) \\ \omega_0 I_1(\omega_0)\end{bmatrix}, \\ \boldsymbol{B}_\sigma(\omega_{\mathrm{c}},\omega_0) &= \begin{bmatrix} B_{\sigma x} \\ B_{\sigma\sigma}\end{bmatrix} = \begin{bmatrix} -\omega_{\mathrm{c}}K_1(\omega_{\mathrm{c}}) & K_0(\omega_{\mathrm{c}}) \\ 2K_1(\omega_{\mathrm{c}})+\omega_{\mathrm{c}}K_0(\omega_{\mathrm{c}}) & -K_1(\omega_{\mathrm{c}})\end{bmatrix}\cdot\begin{bmatrix} I_1(\omega_0) \\ \omega_0 I_0(\omega_0)\end{bmatrix}, \end{aligned}\right\} \tag{3.4}$$

where I_0, K_0, I_1, K_1 are the modified Bessel functions of zero and first order. All of these functions may be computed efficiently and accurately using polynomial approximations (Abramowitz & Stegun 1970). Equation (3.2) may be written in the symbolic form

$$\boldsymbol{M}^{\mathrm{C}} = \sigma_0 \int_0^\infty \begin{bmatrix} F_{xx}\cos(\hat{x}t) & F_{x\sigma}\sin(\hat{x}t) \\ F_{\sigma x}\sin(\hat{x}t) & -F_{\sigma\sigma}\cos(\hat{x}t) \end{bmatrix} \mathrm{d}t, \tag{3.5}$$

where $\boldsymbol{F}$ is a function of $\omega, \omega_0, \omega_{\mathrm{c}}, t$. It may be shown that as t tends to zero, all components of $\boldsymbol{F}$ tend to zero except for the xx-component, $F_{xx} = 8\ln t + \ldots$. Because this is a logarithmic singularity, the corresponding integral in (3.5) is integrable at the origin. On the other hand, as t tends to infinity, and as long as $\sigma < \sigma_{\mathrm{c}}$, $\sigma_0 < \sigma_{\mathrm{c}}$, $\boldsymbol{F}$ decays at the exponential rate $\exp[(\sigma+\sigma_0-2\sigma_{\mathrm{c}})t]$ which guarantees the existence of all integrals in (3.5).

Now, for the purposes of accurate computation, it is imperative to regularize the xx-component of $\boldsymbol{M}^{\mathrm{C}}$. Thus, noting that

$$\int_0^\infty K_0(2\omega_{\mathrm{c}}-\omega-\omega_0)\cos(\hat{x}t)\,\mathrm{d}t = \frac{\pi}{2}\frac{1}{[\hat{x}^2+(2\sigma_{\mathrm{c}}-\sigma-\sigma_0)^2]^{\frac{1}{2}}} \tag{3.6}$$

(Happel & Brenner 1973, p. 303), we write

$$M^{\mathrm{C}}_{xx} = \sigma_0 \int_0^\infty F'_{xx}\cos(\hat{x}t)\,\mathrm{d}t - \frac{4\pi\sigma_0}{[\hat{x}^2+(2\sigma_{\mathrm{c}}-\sigma-\sigma_0)^2]^{\frac{1}{2}}}, \tag{3.7}$$

where

$$F'_{xx} \equiv F_{xx} + 8K_0(2\omega_{\mathrm{c}}-\omega-\omega_0).$$

As t tends to zero, $K_0(2\omega_{\mathrm{c}}-\omega-\omega_0)$ behaves like $-\ln(2\omega_{\mathrm{c}}-\omega-\omega_0)$, and the modified integrand F'_{xx} tends to a finite value. On the other hand, as t tends to infinity, F'_{xx} decays exponentially at the same rate as F_{xx}. In retrospect, the argument of the Bessel function in (3.6) was designed so that as t tends to infinity, F'_{xx} and F_{xx} decay at identical rates.

Next, we consider the Green's function $\boldsymbol{M}^{\mathrm{TA}}$ expressing the flow due to an array of $2N+1$ rings of point forces of separation L, placed coaxially within the tube, where the superscript A stands for *array*. As for the case of a single ring, we decompose $\boldsymbol{M}^{\mathrm{TA}} = \boldsymbol{M}^{\mathrm{RA}} + \boldsymbol{M}^{\mathrm{CA}}$ where $\boldsymbol{M}^{\mathrm{RA}}$ represents flow due to an array of rings of point forces in an infinite fluid, and $\boldsymbol{M}^{\mathrm{CA}}$ is the complementary component. Summing (3.7) we obtain

$$M^{\mathrm{CA}}_{xx} = \sigma_0 \int_0^\infty F'_{xx} \sum_{n=-N}^{N} \cos[(\hat{x}+nL)t]\,\mathrm{d}t - 4\pi\sigma_0 \sum_{n=-N}^{N} \frac{1}{[(\hat{x}+nL)^2+(2\sigma_{\mathrm{c}}-\sigma-\sigma_0)^2]^{\frac{1}{2}}}. \tag{3.8}$$

The sum within the integral in (3.8) may be expressed in closed form using the identity

$$H(N) \equiv \sum_{n=-N}^{N} \exp[\mathrm{i}(\hat{x}+nL)t)] = \exp(\mathrm{i}\hat{x}t)\frac{\cos(NLt)-\cos[(N+1)Lt]}{1-\cos(Lt)}. \tag{3.9}$$

Considering an infinite array of rings, we pass to the limit as N tends to infinity, and obtain

$$H(\infty) = \frac{2\pi}{L}\exp(\mathrm{i}\hat{x}t)\sum_{m=-\infty}^{\infty}\delta\left(t-\frac{2\pi m}{L}\right), \tag{3.10}$$

where δ is the one-dimensional delta function (Lighthill 1958, p. 67). Substituting (3.10) into (3.8) and adding the flow due to the primary rings we obtain we obtain the periodic Green's function

$$M^{\mathrm{TP}}_{xx} = \sigma_0 \frac{2\pi}{L}\left[\tfrac{1}{2}F'_{xx}(t=0) + \sum_{m=1}^{\infty} F'_{xx}(t_m)\cos(t_m\hat{x})\right] + \sum_{n=-\infty}^{\infty}\left[M^{\mathrm{R}}_{xx}(\hat{x}+nL) - \frac{4\pi\sigma_0}{[(\hat{x}+nL)^2+(2\sigma_{\mathrm{c}}-\sigma-\sigma_0)^2]^{\frac{1}{2}}}\right] \quad (3.11)$$

where $t_m = 2\pi m/L$ and the superscript TP stands for tube-periodic. The first sum in (3.11) is convergent, for the individual terms decay at an exponential rate. To demonstrate that the second sum is also convergent, we expand M^{R}_{xx} in an asymptotic series for large values of nL, obtaining

$$M^{\mathrm{R}}_{xx}(\hat{x}+nL) = \frac{2\pi\sigma_0}{[(\hat{x}+nL)^2+(\sigma+\sigma_0)^2]^{\frac{1}{2}}}\left[2 - \frac{(\sigma-\sigma_0)^2}{(\hat{x}+nL)^2+(\sigma-\sigma_0)^2}\right] + \ldots . \quad (3.12)$$

The form of this expansion indicates that the individual terms in the second sum of (3.11) decay like $(nL)^{-2}$, and therefore, this sum is convergent. In practice, in order to compute M^{TP}_{xx}, we truncate the first infinite sum in (3.11) at a value of m such that $2\omega_{\mathrm{c}} - \omega - \omega_0 = 25$, and the second sum at the value $n = 40$.

Repeating the above steps, and noting that $F_{x\sigma}(t=0)$, we obtain

$$M^{\mathrm{TP}}_{x\sigma} = \sigma_0 \frac{2\pi}{L}\sum_{m=1}^{\infty} F_{x\sigma}(t_m)\cos(t_m\hat{x}) + \sum_{n=-\infty}^{\infty} M^{\mathrm{R}}_{x\sigma}(\hat{x}+nL), \quad (3.13)$$

as well as two similar expressions for $M^{\mathrm{TP}}_{\sigma x}$ and $M^{\mathrm{TP}}_{\sigma\sigma}$.

4. Results and discussion

It will be convenient to classify our drops into two categories according to the value of the ratio σ_{c}/a. When $\sigma_{\mathrm{c}}/a > 1$ we have *compact* drops, otherwise we have *elongated* drops. In the limit of large surface tension, compact drops assume a spherical shape, elongated drops tend to adhere to the wall.

4.1. *Compact drops*

First, we illustrate the effect of drop separation, L/a, on the shape of steadily settling drops, fixing the values of σ_{c}/a and Γ. Thus, in figure 2(a–c) we present profiles of steadily settling drops for $\sigma_{\mathrm{c}}/a = 2$, $\Gamma = 0.10$, and $L/a = 6, 3, 2.2$. In all cases, the drops have a slightly prolate shape with a dimpled top. The shape for $L/a = 6$ remains virtually unchanged as L/a is increased beyond this value. As L/a is decreased below 6 one drop starts to feel the presence of its neighbours and obtains an increasingly more elongated shape. In addition, the dimple at the top of each drop becomes more pronounced, and eventually, it yields a fish-tail pattern. Our results indicate that the value $L/a = 2.2$ is very close to the minimum separation corresponding to nearly touching drops and thus it represents the limit of maximum packing.

In figure 3(a–d) we present profiles of steadily settling drops for $\sigma_{\mathrm{c}}/a = 4$, $\Gamma = 0.10$, and $L/a = 6.0, 4.5, 3.2, 3.0$. The drops shown in figure 3(a, b) for $L/a = 6$, 4.5 are slightly prolate with a conical upper end. There is an interesting inversion in shape as L/a is decreased from 4.5 to 3.2; the drops remain slightly prolate but with

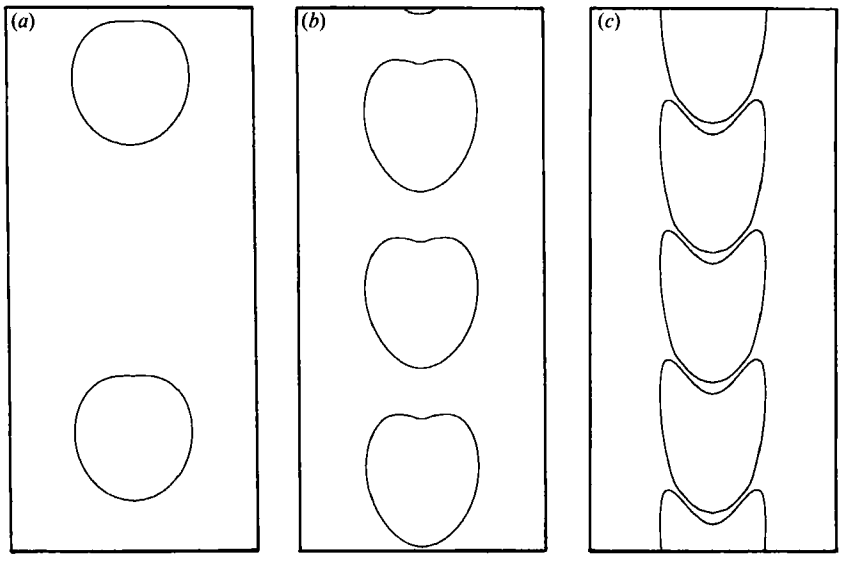

FIGURE 2. Steadily settling drops for inverse Bond number $\Gamma = 0.10$, tube radius $\sigma_c/a = 2.0$ and separation (*a*) $L/a = 6.0$, (*b*) 3.0, (*c*) 2.2.

a conical bottom end. When L/a is decreased below 3.2, the drops develop a dimple at the upper surface as illustrated in figure 3(*d*). This indicates that pronounced dimpling of the top of a drop is characteristic of all closely packed drops independently of the radius of the tube.

In figure 4(*a–c*) we present profiles of steadily moving drops for a larger tube radius $\sigma_c/a = 8$, $\Gamma = 0.10$, and $L/a = 6, 4, 3$. Note that to save space, we have not drawn the wall of the tube. The shape shown in figure 4(*a*) is similar to that shown in figure 3(*a*), and this indicates that for $L/a = 6$, the effect the tube becomes weak when σ_c/a is increased beyond 4. Comparing figure 4(*b*) to figure 3(*b*) we see an interesting variation. For $\sigma_c/a = 8$, as L/a is decreased the dimple at the top of a drop is unstable: ambient fluid enters the drop along the axis of the tube, and the drop obtains a composite prolate shape. After a certain amount of ambient fluid has entered the drop the dimple closes, and the drop reaches a nearly steady state. This behaviour is similar to that of oblate drops settling in an infinite ambient fluid (Pozrikidis 1990). Examining figure 4(*c*) we see that as L/a is reduced to small values, the dimple at the top of the drops is stabilized, and entrainment of ambient fluid is suppressed. This behaviour may be understood by noting that, owing to the dense packing, entrainment would require substantial deformation of the bottom of each drop, but this is prevented by surface tension.

We proceed next to illustrate the effect of drop separation on the terminal velocity of the settling array, U. Thus, in figure 5 we plot the reduced terminal velocity $U^* = U/U_{HR}$ versus a/L for $\Gamma = 0.10$, where U_{HR} is the terminal velocity of a spherical drop settling in an infinite ambient fluid given by Hadamard and Rybzinsky; under our non-dimensionalization, $U_{HR} = 4/15$. Note that the curves in figure 5 end at a value of a/L less than 0.50 which would correspond to touching spherical drops. Figure 5 indicates that for constant σ_c/a, increasing a/L, that is decreasing the separation between the drops, causes the drops to move faster, and this feature becomes more pronounced at high values of σ_c/a. At sufficiently small values of L/a and large values of σ_c/a, the terminal velocity of the drops may well exceed that of solitary drops moving in an infinite ambient fluid.

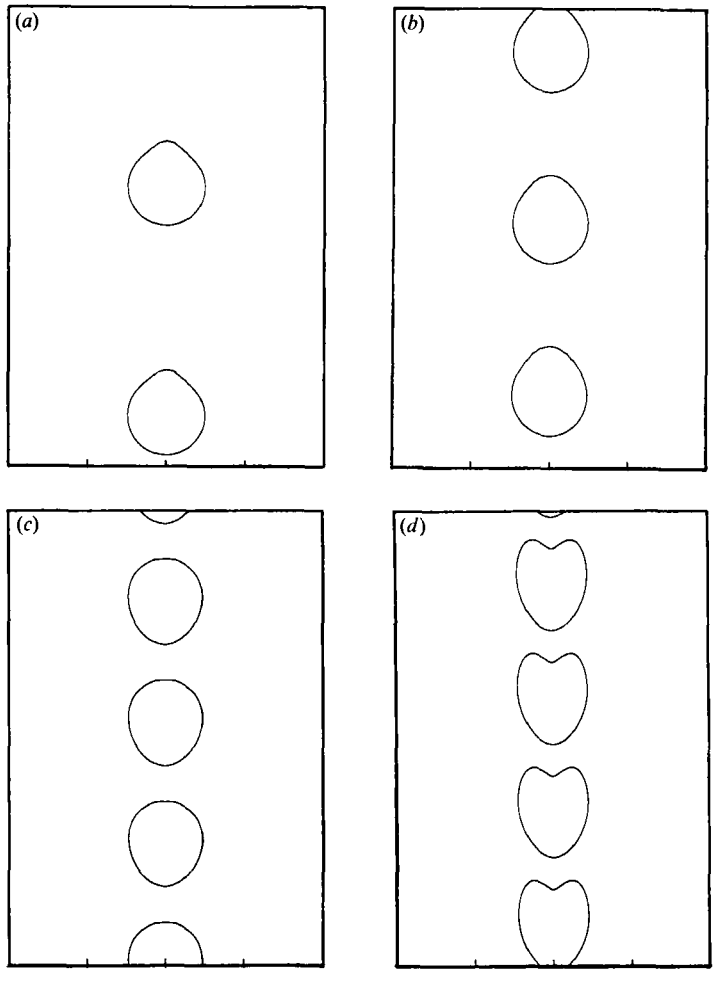

FIGURE 3. Steadily settling drops for $\Gamma = 0.10$, $\sigma_c/a = 4.0$ and separation (*a*) $L/a = 6.0$, (*b*) 4.5, (*c*) 3.2, (*d*) 3.0.

The results presented in figure 5 indicate that in the range $0 < a/L < a/\sigma_c$, U^* is a weak function of a/L which, in turn, implies that the tube introduces a cutoff length, shielding one individual drop from the action of distant drops, i.e. drops that are located more than roughly one tube radius away. This is not surprising, for inspection of the Green's function discussed in §3 reveals that the flow produced by a drop decays at an exponential rate up and down the tube. Based on this observation, we deduce that the number of active drops, N, that is the number of drops that affect the motion of another drop in the array, is proportional to σ_c/L. Recalling that in the absence of the tube the velocity field produced by one drop decays like $1/r$, we find that the magnitude of the velocity at the location of one drop due to the all other drops is proportional to $\log(N)$. This suggests that at sufficiently high values of σ_c/L, U^* is a linear function of $\log(\sigma_c/L)$. When $\sigma_c/a = \infty$, U^* is unbounded for any finite value of a/L, and this indicates that in the limit $\sigma_c/a \to \infty$, the family of curves shown in figure 5 tends to a vertical line that passes through the point $a/L = 0$, $U^* = 1$.

In figure 5 we have also plotted results for perfectly spherical drops or $\Gamma = \infty$, constructed from the data presented by Hyman & Skalak (1972). In the limit of

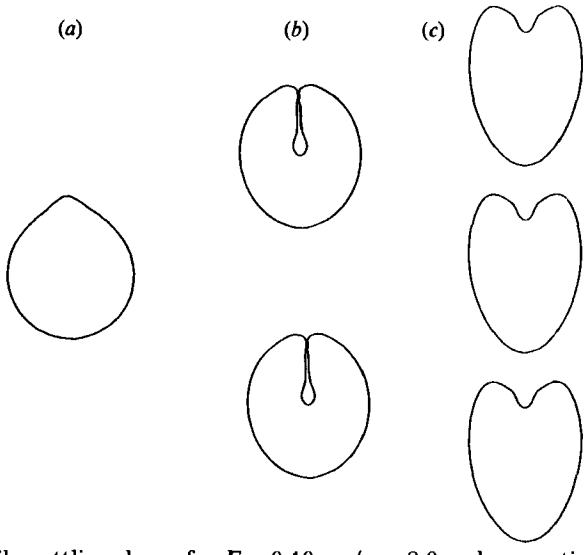

FIGURE 4. Steadily settling drops for $\Gamma = 0.10$, $\sigma_c/a = 8.0$ and separation (*a*) $L/a = 6.0$, (*b*) $L/a = 4.0$, (*c*) $L/a = 3.0$.

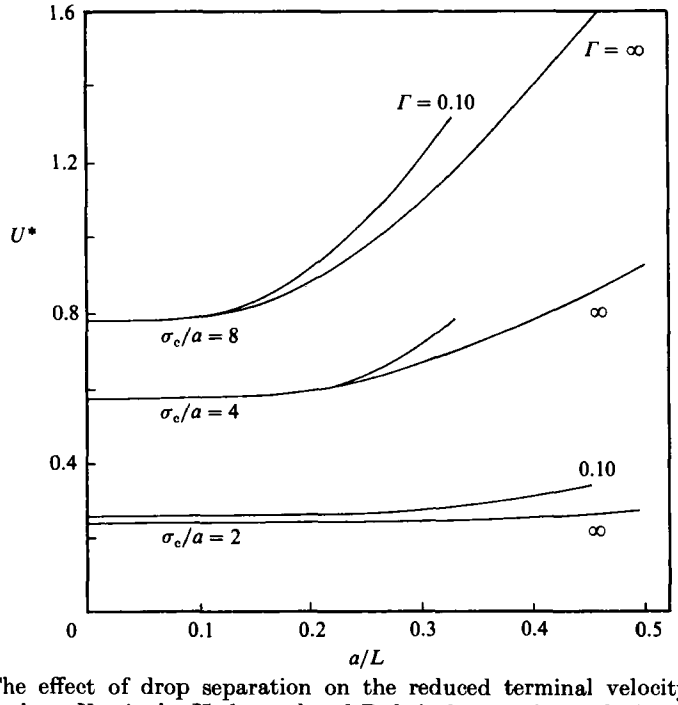

FIGURE 5. The effect of drop separation on the reduced terminal velocity of settling drops, $U^* = U/U_{HR}$ where U_{HR} is the Hadamard and Rybzinsky terminal velocity of a single drop that moves in an infinite ambient fluid. The curves labelled $\Gamma = \infty$ correspond to perfectly spherical drops and were constructed from the results of Hyman & Skalak (1972).

infinite separation, $a/L = 0$, the terminal velocity of the deformed drops is remarkably close to that of perfectly spherical drops, and the difference remains small at finite values of a/L. In all cases, deformed drops move faster than spherical drops.

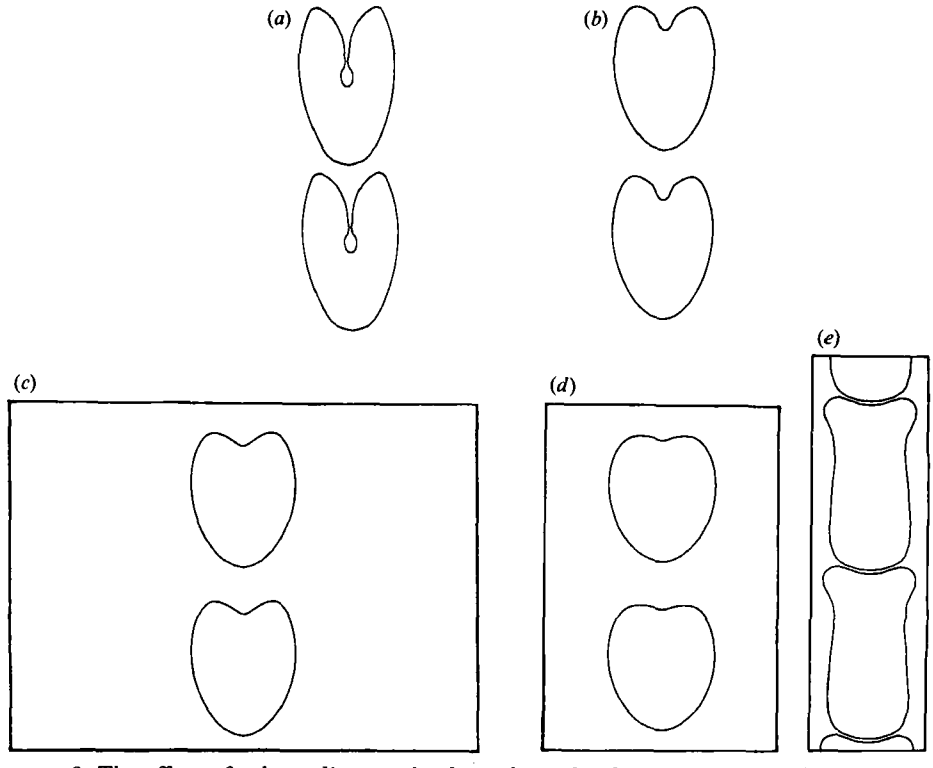

FIGURE 6. The effect of tube radius on the drop shape for drop separation $L/a = 3$. Steadily settling drops for $\Gamma = 0.10$, and (*a*) $\sigma_c/a = 16$, (*b*) 8, (*c*) 4, (*d*) 2, (*e*) 1.

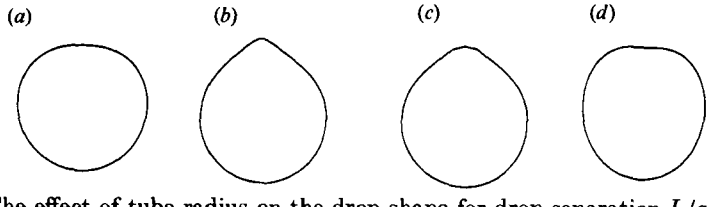

FIGURE 7. The effect of tube radius on the drop shape for drop separation $L/a = 6$. Steadily settling drops for $\Gamma = 0.10$, and (*a*) $\sigma_c/a = 32$, (*b*) 8, (*c*) 4, (*d*) 2.

Examining the motion from a different perspective, we consider now the effect of the tube radius, σ_c/a, maintaining L/a and Γ constant. In figure 6(*a–e*) we present steady drop profiles for $L/a = 3$, $\Gamma = 0.10$, and $\sigma_c/a = 16, 8, 4, 2, 1$. The shape shown in figure 6(*a*) remains unchanged as σ_c/a is increased beyond the value of 16. The main message delivered by figure 6(*a–e*) is that decreasing the radius of the tube has a stabilizing effect on the shape of the drops. When $\sigma_c/a = 1$, the drops are forced to squeeze against each other, attaining a convoluted shape. It should be noted that the profile shown in figure 6(*e*) is nearly but not entirely steady, but the slow evolution beyond the stage shown in this figure could not be described with sufficient accuracy with our numerical procedure.

In figure 7(*a–c*) we present drop profiles for $\sigma_c/a = 32$, 8, 4, 2 and $L/a = 6$, $\Gamma = 0.10$. It is interesting to note that increasing σ_c/a above 2 causes the top of a drop to change its shape from slightly dimpled, to prolate with a conical upper end, to flat, and eventually, to slightly dimpled.

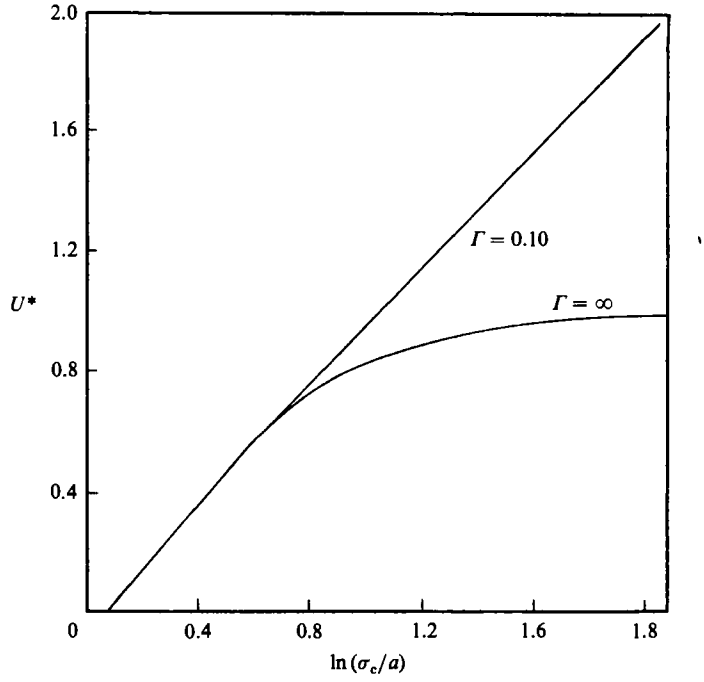

FIGURE 8. The effect of tube radius on the reduced settling velocity U^*. The curve labelled $\Gamma = \infty$ corresponds to perfectly spherical drops and was constructed from the results of Hyman & Skalak (1972) and Coutanceau & Thizon (1981).

To illustrate the effect of σ_c/a on the terminal drop velocity, in figure 8, we plot U^* for the drops shown in figure 7 versus $\log(\sigma_c/L)$ on a semilogarithmic scale. We observe nearly linear behaviour, which is in agreement with our previous arguments regarding the relation between U^* and σ_c/a. In the same plot we show the reduced terminal velocity of perfectly spherical solitary drops, $\Gamma = \infty$, constructed using the data of Hyman & Skalak (1972) and Coutanceau & Thizon (1981). Note that when σ_c/L is less than L/a, the velocity of the periodic drops is remarkably close to that of solitary spherical drops (within one percent), indicating that the effects of drop deformation and interaction are negligible. As σ_c/L is increased beyond L/a, the velocity of the periodic drops tends to become unbounded, whereas that of the solitary drops tends to U_{HR}.

So far we have examined the effect of the geometrical ratios σ_c/L and L/a, maintaining the inverse Bond number, Γ, constant. Next we examine the effect of Γ, and at the same time illustrate the nature of transient drop evolution. In figure 9(*a–c*) we present three sequences of evolving drops for $L/a = 2\pi$, $\sigma_c/a = 2.50$, 1.50, 1.10, and $\Gamma = 0$. In all three cases, at the initial instant, the drops have a spherical shape. During the early stages of motion, all drops flatten at the top forming an axisymmetric dimple. Ambient fluid is entrained through the dimple into the drop along the axis, amplifying the dimple. The subsequent evolution depends strongly upon the radius of the tube.

The evolution of the drop for $\sigma_c/a = 2.50$ shown in figure 9(*a*), is qualitatively similar to that of an oblate drop settling in an infinite ambient fluid (Kojima *et al.* 1984; Pozrikidis 1990). This entails convection of the entrained ambient fluid up to the bottom of the drop, reduction of the drop into a translating drop ring, and

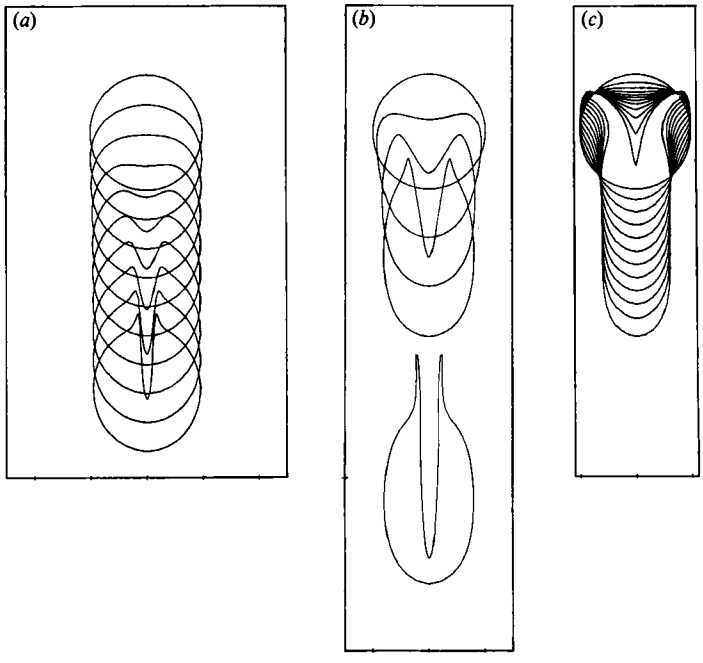

FIGURE 9. Evolving drops profiles of initially spherical drops for vanishing surface tension, $\Gamma = 0$; (a) $\sigma_c/a = 2.5$, time increases in intervals of 5 from 0 to 45; (b) $\sigma_c/a = 1.5$, $t = 0$, 20, 40, 60.5, 80, 90.5; for clarity, the last frame has been shifted down by 3 units; (c) $\sigma_c/a = 1.10$, $t = 0$, 10, 20, 30, 40, 50, 60, 70, 80, 90, 100.5, 114.5.

ejection of an axisymmetric filament from the top of the drop. The evolution of the drop for $\sigma_c/a = 1.50$, shown in figure 9(*b*) follows a pattern similar to that for $\sigma_c/a = 2.50$, with the most notable variation the prolate shape of the main body of the drop. The evolution of the drop for $\sigma_c/a = 1.10$, shown in figure 9(*c*), shows a novel and intriguing feature: at large times, the ejected tail develops a fish-like shape. This behaviour may be understood by observing that as the drop is settling, ambient fluid is convected upwards through the narrow annular gap that develops between the drop and the tube. This fluid pushes the tail of the drop toward the centre of the tube, causing it to close upon itself at large times.

Figure 9 suggests that in the absence of surface tension, settling drops transform into translating prolate rings that undergo some degree of filamentation. To illustrate the effect of surface tension, in figure 10(*a–c*) we present three patterns of evolution corresponding to those shown in figure 9(*a–c*), but with finite surface tension, $\Gamma = 0.10$. A marked change in behaviour is now apparent: filamentation is suppressed, and the drops acquire a steady prolate shape in a smooth manner. The aspect ratio of the asymptotic shape is affected drastically by the radius of the tube, and is equal to 1.07 for $\sigma_c/a = 2.50$, 1.38 for $\sigma_c/a = 1.50$, and 3.06 for $\sigma_c/a = 1.10$.

To illustrate the nature of the flow inside and outside the drops, in figure 10(*d*) we present the streamline pattern at steady motion for $\sigma_c/a = 1.10$ in a frame of reference moving with the terminal velocity of the drop. The streamlines on either side of the boundary of the drop are nearly parallel to the contour of the drop confirming that, indeed, the drop has reached a steady state. There is a single toroidal viscous eddy occupying the whole volume of the drop, and no eddy in the exterior of the drop. These features are in general agreement with the experimental

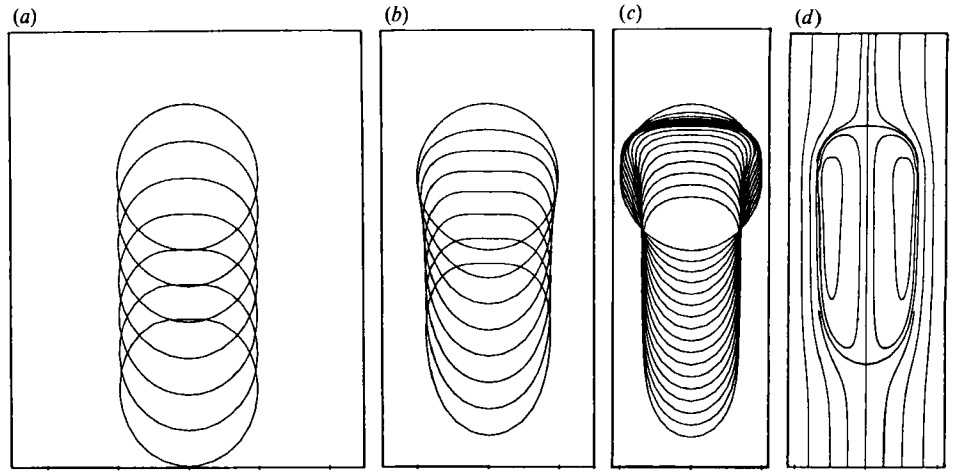

FIGURE 10. The effect of tube radius on the evolution of initially spherical drops. Evolving drop profiles for $\Gamma = 0.10$; (*a*) $\sigma_c/a = 2.5$, time increases in intervals of 5 from 0 to 45; (*b*) $\sigma_c/a = 1.5$, time increases in intervals of 10 from 0 to 70; (*c*) $\sigma_c/a = 1.10$, time increases in intervals of 10 from 0 to 160. (*d*) Streamline pattern in a frame of reference moving with the drop for the profile corresponding to the latest time shown in (*c*).

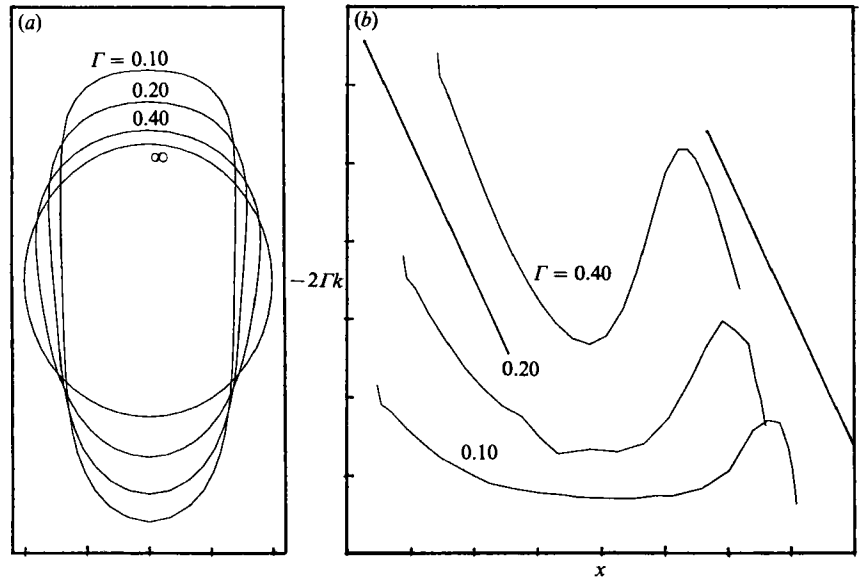

FIGURE 11. The effect of surface tension: (*a*) profiles of steadily moving drops for $\sigma_c/a = 1.10$, and $\Gamma = 0.10, 0.20, 0.40, \infty$, placed with common centre of gravity; (*b*) the corresponding distribution of capillary versus gravitational forces along the boundary of the drops for $\Gamma = 0.10, 0.20, 0.40$; linear behaviour (indicated by the straight lines) suggests that viscous forces are insignificant.

observations of Goldsmith & Mason (1962). The fact that the flow becomes rectilinear a short distance above and below the drop suggests that the behaviour of one drop is virtually independent of the presence of the other drops in the settling array.

It is intuitively evident that increasing the surface tension will cause the drops to obtain a more compact shape. To illustrate this feature, in figure 11 (*a*) we present four steady drop shapes for $\sigma_c/a = 0.10, L/a = 2\pi$, and $\Gamma = 0.10, 0.20, 0.40$, as well the

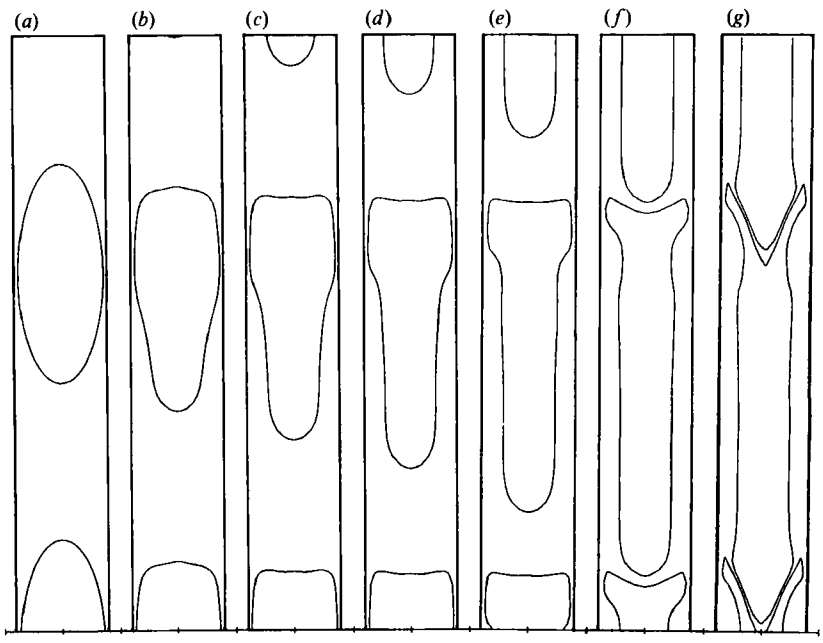

FIGURE 12. A sequence of evolving profiles of a spheroidal drop settling inside a tube of $\sigma_c/a = 0.80$, for vanishing surface tension $\Gamma = 0$ and $L/a = 2\pi$ at $t = 0$, 40, 80, 120, 180, 270, 330 (a–g).

asymptotic spherical shape corresponding to $\Gamma = \infty$. The deviation from sphericity is moderate for $\Gamma = 0.40$, but pronounced at lower values of Γ. The reduced settling velocity is a strong function of Γ, and decreases from $U^* = 0.0170$ for $\Gamma = 0.10$, to $U^* = 0.0115$ for $\Gamma = 0.20$, to $U^* = 0.00450$ for $\Gamma = 0.40$.

To gain insight into the nature of the flow around the drops shown in figure 11(a), we consider the relative strength of the three forces governing the motion of the fluid: viscous forces, gravitational forces, and surface tension. To assess the relative magnitude of these forces, in figure 11(b) we plot the capillary force, $-2\Gamma k$, versus the gravitational surface force x around the contour of the drop for the three cases $\Gamma = 0.10$, 0.20, 0.40. A slope of -1 indicates that surface tension and gravitational forces balance and viscous forces are insignificant. We thus see that viscous forces are negligible at the top and at the bottom of the drop for the two cases $\Gamma = 0.20$, 0.40, but make significant contributions in the intervening regions along the side of the drops.

4.2. *Elongated drops*

In the second part of our investigation we consider the behaviour of elongated drops with $\sigma_c/a < 1.0$. Beginning our illustration, we present a sequence of evolving profiles of an initially spheroidal drop with aspect ratio 2.5, for $\sigma_c/a = 0.80$, $L/a = 2\pi$, and $\Gamma = 0$ (figure 12(a–g). We observe that during the early stages of motion, the bottom of each drop elongates while the top tends to become flat (figure 12a–c). As time progresses, the top remains nearly immobile while the bottom assumes the shape of a nearly cylindrical finger (figure 12d, e). It is interesting to observe the onset of an interfacial front that propagates along the side of each drop and causes the gap between the side of the drop and the tube to increase progressively from bottom to top. At large times, the continuous elongation of the drops leads to collision and partial dispersion of the drop fluid into the ambient fluid

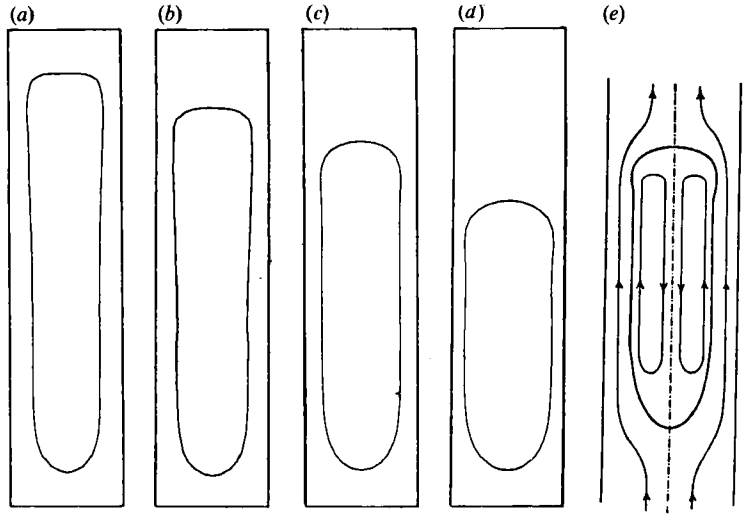

FIGURE 13. Profiles of steadily settling drops for $\sigma_c/a = 0.80, L/a = 2\pi$, for (*a*) $\Gamma = 0.025$, (*b*) 0.05, (*c*) 0.10, (*d*) 0.205. The panel (*e*) illustrates a schematic drawing presented by Goldsmith & Mason (1962, figure 2).

(figure 6*f*, *g*). Summarizing the evolution, we may state that the initial array of spheroidal drops is unable to sustain its structure, but transforms into a cylindrical core which is settling along the axis of the tube.

Next, we examine the effect of surface tension, maintaining all other parameters constant. Our computations show that the transient evolution of drops with finite surface tension is similar to that of compact drops. In figure 13(*a*–*d*) we present a family of steady drops shapes for $\sigma_c/a = 0.80$, $L/a = 12$, and $\Gamma = 0.025$, 0.05, 0.10, 0.20. All drops are composed of a nearly cylindrical body and two curved ends. The curvature of the top increases, whereas that of the bottom decreases as Γ is increased. Clearly, increasing Γ reduces the length of the drops and, consequently, the size of the gap between the drops and the tube. The overall shape of the drops shown in figure 13(*a*–*d*) is similar to that shown in figure 13(*e*) which was drawn by Goldsmith & Mason (1962) according to their laboratory observations.

It has been noted by several previous authors that the terminal velocity of an elongated drop will depend primarily on the radius of the tube and the physical properties of the fluids, and will be insensitive to the length or volume of the drop. To derive an expression for the terminal velocity of a drop, Goldsmith & Mason (1962) noted that the flow over the main body of an elongated drop is virtually unidirectional. Requiring that the pressure does not change in the radial direction regardless of the magnitude of surface tension, they derived a relationship between the reduced terminal velocity $V = \mu U/\Delta\rho g\sigma_c^2$ and the reduced radius of the cylindrical body of the drop, $\beta = \sigma_{max}/\sigma_c$. Rearranging their equations (11)–(15) yields

$$V = -\frac{1}{8}\frac{\beta^2}{\beta^4+\lambda(1-\beta^4)}\{1-4\beta^2+3\beta^4-4\beta^4\ln\beta-4\lambda(1-\beta^2)[(1+\beta^2)\ln\beta+(1-\beta^2)]\}, \tag{4.1}$$

where μ is the viscosity of the suspending fluid and $\lambda\mu$ is the viscosity of the drop. Our numerical results corroborate the validity and accuracy of the theory of Goldsmith & Mason. Our computed velocity profiles across the main body of the

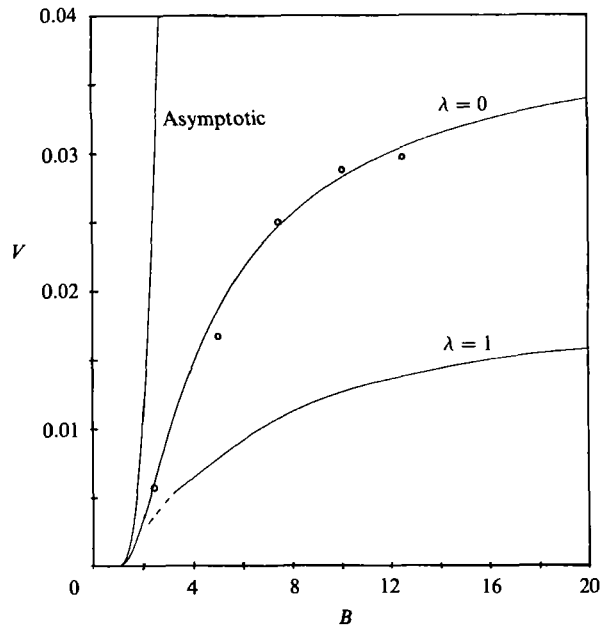

FIGURE 14. The reduced terminal velocity of an elongated drop $V = \mu U/\Delta\rho g\sigma_c^2$ as a function of the tube Bond number $B = \Delta\rho g\sigma_c^2/\gamma$. The curve labelled $\lambda = 1$ shows the results of the present study; the curve labelled *Asymptotic* shows the results of Bretherton (1961) for tightly fitting inviscid drops, $\lambda = 0$; the curve labelled $\lambda = 0$ shows the numerical results of Reinelt (1987) for inviscid fingers, $\lambda = 0$; the discrete data points corresponding to the measurements of Goldsmith & Mason (1962, figure 3) for $\lambda = 0$.

elongated drops were in excellent agreement with those predicted by the theory of Goldsmith & Mason, and the terminal velocity was predicted quite accurately, within a few percent, by equation (4.1).

Now, it is evident that the value of β must be known before (4.1) can be used to compute V. On the grounds of dimensional analysis, one may argue that β is a function of the viscosity ratio λ and the tube Bond number $B = \Delta\rho g\sigma_c^2/\gamma$, implying that V is a function of λ and B. Unfortunately, there is no available theory relating β to λ and B, except for the case $\lambda = 0$ and in the limit of a narrow gap, $\beta \to 1$ or $\delta = \beta - 1 \to 0$, where

$$B = 0.842 + 1.10\delta^{\frac{2}{3}} + 1.85\delta + \ldots \tag{4.2}$$

(Bretherton 1961). Clearly, when $B = 0.842$, $\delta = 0$ and the gap closes, halting the motion of the fluid. Combining (4.1) and (4.2) yields a relationship between V and B,

$$B = 0.842 + 1.25Ca^{\frac{2}{3}} + 2.24Ca^{\frac{1}{3}} + \ldots, \tag{4.3}$$

where $Ca = VB = \mu U/\gamma$ is the capillary number. In our computations we seek to establish the precise dependence of V and β on B for $\lambda = 1$.

In figure 14 we present a plot of V versus B including our numerical results for $\lambda = 1$, the numerical results of Reinelt (1987) for $\lambda = 0$, the data of Goldsmith & Mason (1962, figure 3) for $\lambda = 0$, and the asymptotic results of Bretherton (1961) expressed by equation (4.3). Considering first the case $\lambda = 0$, we see a good agreement between the numerical results and the experimental data; the slight discrepancies might be attributed to experimental difficulties, including the presence of impurities, ambiguities in measuring surface tension, or finite size of the generated drops. The asymptotic theory of Bretherton (1961) is consistent with the numerical and

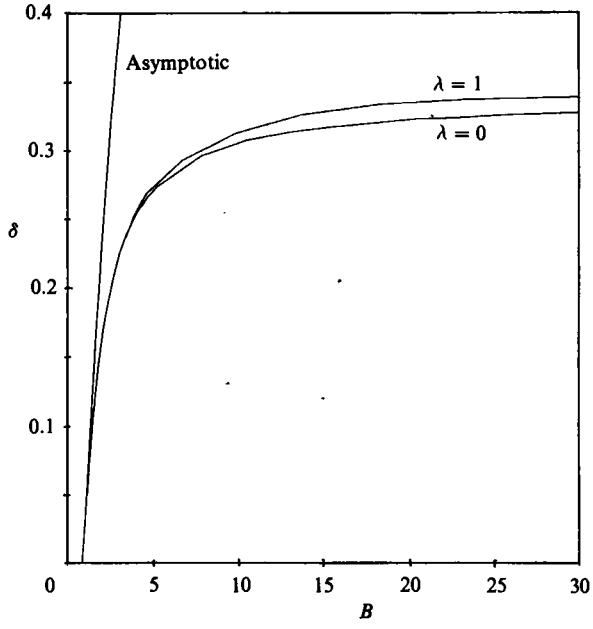

FIGURE 15. The reduced gap of an elongated drop, δ, as a function of the tube Bond number, B. The curve labelled $\lambda = 1$ shows the results of the present study; the curve labelled *Asymptotic* shows the results of Bretherton (1961) for tightly fitting inviscid drops, $\lambda = 0$; the curve labelled $\lambda = 0$ shows the numerical results of Reinelt (1987).

experimental results near the critical Bond number $B_{cr} = 0.842$, but grossly overpredicts the terminal velocity at larger values of B. Inspecting next our results, we find that the velocity of drops with $\lambda = 1$ is roughly half that of inviscid drops. As B is increased, V tends to an asymptotic limit corresponding to drops with vanishing surface tension. This behaviour is consistent with the experimental observations of Barr (1926) who noted that when B is larger than 10, V is virtually independent of B. The V–B curves for values of λ between 0 and 1 are expected to lie between those for $\lambda = 0$ and 1 shown in figure 14.

Results for values of B near B_{cr} were prohibited by two pragmatic constraints: the time step had to be reduced in order to maintain numerical stability, and the accurate computation of the Green's function required an excessive computational time. One may argue, however, that equations (4.2) and (4.3) which were derived originally for inviscid drops, $\lambda = 0$, apply also for viscous drops with small or moderate values of λ. This becomes evident by noting that the theory of Bretherton is based on three assumptions: the bottom and top of the drops have a nearly hydrostatic shape; the flow within the gap between the drop and the tube is described by the equations of lubricating flow; the shear stress on the surface of a drop is equal to zero. The first two assumptions are expected to be true in the case of viscous drops. To see that the third assumption is also valid, we note that the ratio of the interfacial shear stress on the side of the drop to that on the side of the suspending fluid is of order $\lambda\beta$, which is a small number provided that λ is not excessively large. Certainly, the critical value $B_{cr} = 0.842$ will be applicable for any value of λ.

We proceed next to consider the relationship between the reduced gap δ and the Bond number B. In figure 15 we present our results for $\lambda = 1$, those of Reinelt (1987) for $\lambda = 0$, and the predictions of the asymptotic analysis of Bretherton (1961) for

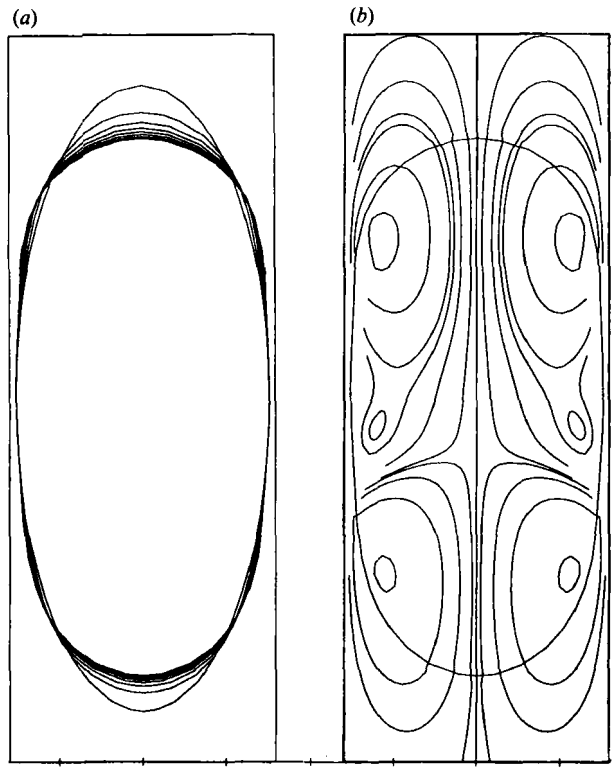

FIGURE 16(*a*). Successive stages in the evolution of an initially spheroidal drop with aspect ratio 2.25 and $\Gamma = 1.0$ or $B = 0.640$, at times $t = 0, 3, 6, \ldots, 21$; (*b*) instantaneous streamline pattern at $t = 21$.

$\lambda = 0$ expressed by equation (4.2). We observe that as the viscosity of the drop is increased from $\lambda = 0$ to 1 the gap between the drop and the tube increases but only by a small amount. At values of B near B_{cr} our results agree with those of Reinelt and Bretherton, and this corroborates our previous argument that when the gap is small, the viscosity of the drop plays a secondary role in determining the shape and behaviour of the drop.

Bretherton (1961) found that at values of B below 0.842, steady translation is not possible, and the drops must move unsteadily, break up into smaller fragments, or adhere to the wall. The prevailing type of behaviour will depend upon the initial shape of the drop. For instance, it is conceivable that very slender drops will tend to contract, breaking up into a number of droplets. Experiments indicate that drops with a moderate aspect ratio will follow a different protocol of evolution (O'Brien 1969) which is exemplified in figure 16(*a*) for an initially spheroidal drop with aspect ratio 2.25 and $\Gamma = 1.0$ or $B = 0.640$. We observe that the top and bottom of the drop tend to contract under the action of capillary forces, forcing the sides of the drop against the tube. Instead of settling, the drop tends to attain a hydrostatic configuration which is composed of a stationary upper and a lower meniscus and a cylindrical main body. The long-time behaviour of the drop may be visualized by inspecting the instantaneous streamline pattern depicted in figure 16(*b*). Note that the absence of fore-and-aft symmetry is due to the effect of gravity. The eddies at the upper and lower menisci promote the contraction of the drop at either end, and the drainage of suspending fluid through the narrow gap between the drop and the tube.

There are too small toroidal eddies near the mid-plane of the drop; the eddy which is attached to the wall causes the side of drop to deform and break up into lenticular fragments. This process of breakup has been analysed by Goren (1964) in the context of linear stability analysis, by Hammond (1983) in the context of lubrication theory, and by Newhouse & Pozrikidis (1991) in the context of nonlinear stability analysis.

The author would like to express his appreciation to Professor D. Reinelt for providing him with numerical values of his computations, and to Dr V. O'Brien for making available a copy of her technical memorandum. This work has been supported by the National Science Foundation, Grant CTS-9020728.

REFERENCES

ABRAMOWITZ, M. & STEGUN, I. A. 1970 *Handbook of Mathematical Functions.* Dover.

ABRAMS, V. R., KAVANAGH, J. T. & OSMOND, C. H. 1921 Air bubble viscometer. *Chemical Metall. Engng* **25**, 665–666.

BARR, G. 1926 The air-bubble viscometer. *Phil. Mag.* **1**, 395–405.

BATCHELOR, G. K. 1967 *An Introduction to Fluid Dynamics.* Cambridge University Press.

BRETHERTON, F. P. 1961 The motion of long bubbles in tubes. *J. Fluid Mech.* **10**, 166–188.

CLIFT, R., GRACE, J. R. & WEBER, M. E. 1978 *Bubbles, Drops, and Particles.* Academic.

COUTANCEAU, M. & THIZON, P. 1981 Wall effects on the bubble behaviour in highly viscous liquids. *J. Fluid Mech.* **107**, 339–373.

FAUST, O. 1919 Viskositätsmessungen. *Z. Phys. Chem.* **93**, 758–761.

GOLDSMITH, H. L. & MASON, S. G. 1962 The movement of single large bubbles in closed vertical tubes. *J. Fluid Mech.* **14**, 42–58.

GOLDSMITH, H. L. & MASON, S. G. 1963 The flow of suspensions through tubes II. Single large bubbles. *J. Colloid Sci.* **18**, 237–261.

GOREN, S. L. 1964 The shape of a thread of liquid undergoing break-up. *J. Colloid Sci.* **19**, 81–86.

HABERMAN, W. L. & SAYRE, R. M. 1958 Motion of rigid and fluid spheres in stationary and moving liquids inside cylindrical tubes. *David Taylor Model Basin Rep.* 1143.

HAMMOND, P. S. 1983 Nonlinear adjustment of a thin annular film of viscous fluid surrounding a thread of another within a circular cylindrical pipe. *J. Fluid Mech.* **137**, 363–384.

HAPPEL, J. & BRENNER, H. 1973 *Low Reynolds Number Hydrodynamics.* Martinus Nijhoff.

HE, Z., DAGAN, Z. & MALDARELLI, C. 1991 The influence of surfactant adsorption on the motion of a fluid sphere in a tube. Part 1. Uniform retardation controlled by sorption kinetics. *J. Fluid Mech.* **222**, 1–32.

HETSRONI, G., HABER, S. & WACHOLDER, E. W. 1970 The flow fields in and around a droplet moving axially within a tube. *J. Fluid Mech.* **41**, 689–705.

HYMAN, W. A. & SKALAK, R. 1972 Viscous flow of a suspension of liquid drops in a cylindrical tube. *Appl. Sci. Res.* **26**, 27–52.

KENNEDY, M. 1991 Numerical investigations of the dynamics of three-dimensional drops. Ph.D. thesis, University of California at San Diego.

KOJIMA, M., HINCH, E. J. & ACRIVOS, A. 1984 The formation and expansion of a toroidal drop moving in a viscous fluid. *Phys. Fluids* **27**, 19–32.

LIGHTHILL, M. J. 1958 *An Introduction to Fourier Analysis and Generalised Functions.* Cambridge University Press.

LISTER, J. R. 1989 Selective withdrawal from a viscous two-layer system. *J. Fluid Mech.* **198**, 231–254.

MAO, Z.-S. & DUKLER, A. E. 1990 The motion of Taylor bubbles in vertical tubes. I. A numerical simulation for the shape and rise velocity of Taylor bubbles in stagnant and flowing liquid. *J. Comp. Phys.* **91**, 132–160.

MARTINEZ, M. J. & UDELL, K. S. 1990 Axisymmetric creeping motion of drops through circular tubes. *J. Fluid Mech.* **210**, 565–591.

NEWHOUSE, L. A. & POZRIKIDIS, C. 1991 The instability of annular layers and liquid threads. *UCSD Research Manuscript.*

O'BRIEN, 1969 Large circulating drops in vertical tubes. *Tech. Mem. Applied Physics Laboratory, The Johns Hopkins University.*

POZRIKIDIS, C. 1990 The instability of a moving viscous drop. *J. Fluid Mech.* **210**, 1–21.

POZRIKIDIS, C. 1991 *Boundary Integral and Singularity Methods for Linearized Viscous Flow.* Cambridge University Press.

RALLISON, J. M. 1981 A numerical study of the deformation and burst of a viscous drop in an extensional flow. *J. Fluid Mech.* **109**, 465–482.

RALLISON, J. M. 1984 The deformation of small viscous drops and bubbles in shear flows. *Ann. Rev. Fluid. Mech.* **16**, 45–66.

RALLISON, J. M. & ACRIVOS, A. 1978 A numerical study of the deformation and burst of a viscous drop in an extensional flow. *J. Fluid Mech.* **89**, 191–200.

REINELT, D. A. 1987 The rate at which a long bubble rises in a vertical tube. *J. Fluid Mech.* **175**, 557–565.

TÖZEREN, H. 1984 Boundary integral equation method for some Stokes flow problems. *Intl J. Numer. Meth. Fluids* **4**, 159–170.

WESTBORG, H. & HASSAGER, O. 1989 Creeping motion of long bubbles and drops in capillary tubes. *J. Colloid Interface Sci.* **133**, 135–147.